Fossil and Non-Fossil Sources of Organic and Elemental Carbon Aerosols in the Outflow from Northeast China

Article *in* Environmental Science and Technology · May 2016

DOI: 10.1021/acs.est.6b00351

CITATION
1

READS
105

6 authors, including:

Yanlin Zhang
Nanjing University of Information Science & Technology
44 PUBLICATIONS **716** CITATIONS

SEE PROFILE

Environmental Science & Technology

Article

pubs.acs.org/est

Fossil and Nonfossil Sources of Organic and Elemental Carbon Aerosols in the Outflow from Northeast China

Yan-Lin Zhang,[*,†,‡] Kimitaka Kawamura,[*,‡] Konstantinos Agrios,[§,∥] Meehye Lee,[⊥] Gary Salazar,[§] and Sönke Szidat[§]

[†]Yale-NUIST Center on Atmospheric Environment, Nanjing University of Information Science and Technology, Nanjing 10044, China

[‡]Institute of Low-Temperature Science, Hokkaido University, N19 W08, Kita-ku, Sapporo 060-0819, Japan

[§]Department of Chemistry and Biochemistry & Oeschger Centre for Climate Change Research, University of Bern, Bern 3012, Switzerland

[∥]Paul Scherrer Institute (PSI), Villigen-PSI 5232, Switzerland

[⊥]Department of Earth and Environmental Sciences, Korea University, Seoul 136-701, South Korea

Supporting Information

ABSTRACT: Source quantification of carbonaceous aerosols in the Chinese outflow regions still remains uncertain despite their high mass concentrations. Here, we unambiguously quantified fossil and nonfossil contributions to elemental carbon (EC) and organic carbon (OC) of total suspended particles (TSP) from a regional receptor site in the outflow of Northeast China using radiocarbon measurement. OC and EC concentrations were lower in summer, representing mainly marine air, than in other seasons, when air masses mostly traveled over continental regions in Mongolia and northeast China. The annual-mean contribution from fossil-fuel combustion to EC was 76 ± 11% (0.1−1.3 $\mu g\ m^{-3}$). The remaining 24 ± 11% (0.03−0.42 $\mu g\ m^{-3}$) was attributed to biomass burning, with slightly higher contribution in the cold period (∼31%) compared to the warm period (∼21%) because of enhanced emissions from regional biomass combustion sources in China. OC was generally dominated by nonfossil sources, with an annual average of 66 ± 11% (0.5−2.8 $\mu g\ m^{-3}$), approximately half of which was apportioned to primary biomass-burning sources (34 ± 6%). In winter, OC almost equally originated from primary OC (POC) emissions and secondary OC (SOC) formation from fossil fuel and biomass-burning sources. In contrast, summertime OC was dominated by primary biogenic emissions as well as secondary production from biogenic and biomass-burning sources, but fossil-derived SOC was the smallest contributor. Distinction of POC and SOC was performed using primary POC-to-EC emission ratios separated for fossil and nonfossil emissions.

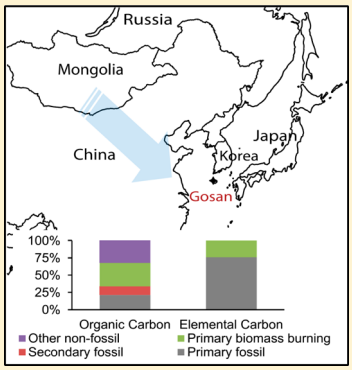

1. INTRODUCTION

Carbonaceous aerosols contribute 10−70% to the atmospheric fine-particulate matter[1,2] and have multiple and significant impacts on air quality, atmospheric visibility, human health, and the Earth's climate.[3−5] The total content of carbonaceous aerosols (i.e., total carbon, TC) is operationally classified into two major fractions, namely organic carbon (OC) and elemental carbon (EC) or black carbon (BC).[6] OC can be directly emitted as primary OC (POC) or formed as secondary OC (SOC) via gas-particle conversion resulting from atmospheric oxidation of anthropogenic and natural precursors.[6,7] OC can affect the Earth's climate forcing by directly reflecting incoming sunlight and indirectly by altering the ability of organic aerosols to act as cloud-condensation nuclei (CCN).[5] EC almost exclusively derives from incomplete combustion of fossil fuel (e.g., coal and petroleum) or biomass,[6,8] leading overall to a warming effect by either absorbing incoming solar radiation or reducing the albedo of the Earth's surface (i.e., snow and ice).[5]

High mass concentrations of carbonaceous particles have been reported in the outflow regions of Chinese pollutants, such as Japan and Korea, due to long-range atmospheric transport.[9−11] Previous studies have also revealed that OC and EC in source regions of China often differ in their origins and formation processes, which may complicate the source identification of aerosols from downwind areas. Therefore, there is an urgent need to get a better understanding of the sources of OC and EC in outflow regions of China. Radiocarbon (^{14}C) analysis is a powerful and unambiguous tool for quantitatively determining fossil versus nonfossil sources of carbonaceous aerosols, especially if such analysis is conducted separately for different carbonaceous fractions such as OC, EC and water-soluble OC (WSOC).[12−14] A recent ^{14}C-

Received: January 24, 2016
Revised: May 17, 2016
Accepted: May 20, 2016

DOI: 10.1021/acs.est.6b00351
Environ. Sci. Technol. XXXX, XXX, XXX−XXX

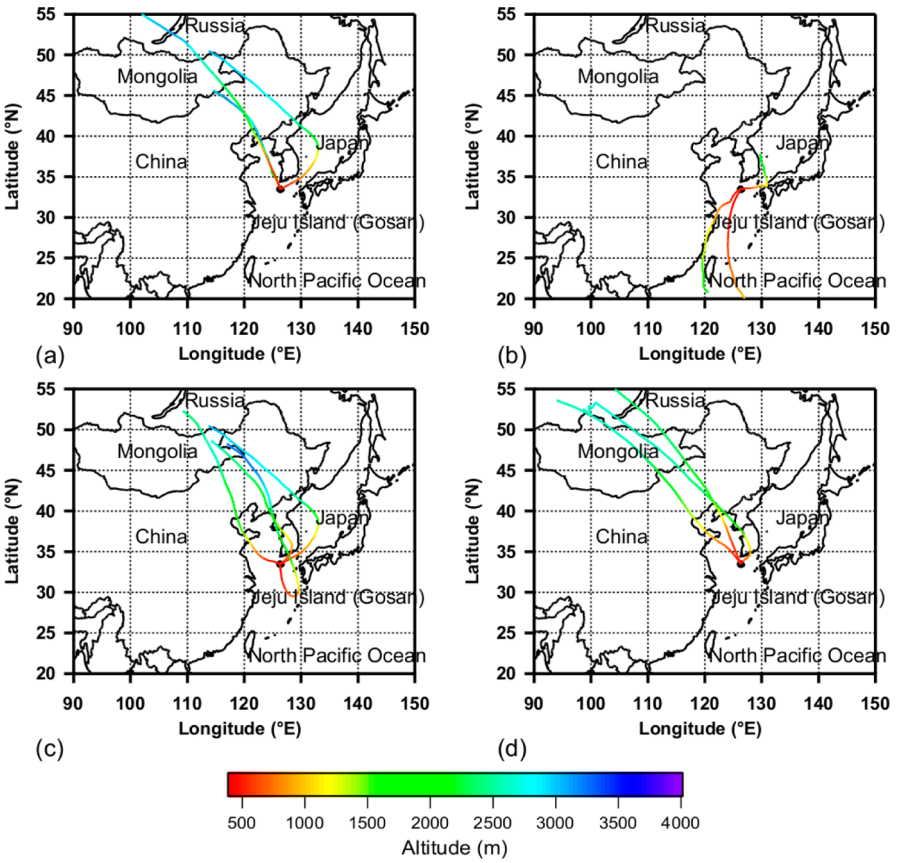

Figure 1. Clustered mean five-day trajectories reaching the sampling site at Gosan, Jeju Island, Korea during spring (panel a, March, April, and May), summer (panel b, June, July, and August), autumn (panel c, September, October, and November), and winter (panel d, December, January, and February) from April 2013 to April 2014.

based source apportionment study showed that fossil sources contribute on average 80% to EC at Gosan site, which is higher than suggested by bottom-up approaches due to less constrains on emission ratios in various fuel types and combustion efficiencies.[15] However, such source constraints are only limited to shorter campaigns or specific seasons.

In this study, ^{14}C measurement combined with the Latin hypercube sampling (LHS) model was applied to aerosol samples from an East Asian receptor site (Gosan supersite at Jeju Island, Korea) to obtain fruitful information on regionally integrated sources and formation processes of carbonaceous aerosols from China. To the best of our knowledge, this is the first time that ^{14}C-based source apportionment was carried out on both EC and OC aerosols in East Asian continental outflow regions, covering a full seasonal cycle.

2. EXPERIMENTAL SECTION

2.1. Sampling. Field sampling was conducted at the Korea Climate Observatory at Gosan, an East Asian Supersite (33.17° N, 126.10° E; see Figure 1), which is located on the western edge of Jeju Island facing the Asian continent (~100 km south of the Korean Peninsula, ~500 km east of China, ~200 km west of Kyushu Island, Japan), and the sampling site is far away from local residential areas of the island. This sampling site has been used in several multinational projects for aerosol studies such as ABC (Atmospheric Brown Clouds) Project[10] and ACE-Asia (Aerosol Characterization Experiment Asia) project[16] as a downwind site of air pollution outflow from the Asian continent.[14,17−19] Total suspended particles (TSP) were collected on preheated (450 °C for at least 6 h) quartz fiber filters (20 cm × 25 cm, Pallflex) using a high-volume air sampler (Kimoto AS-810, ~65 $m^3\ h^{-1}$) near-continuously from April 2013 to April 2014 on the roof of a trailer house (~3 m above the ground). Similar TSP sampling approaches (instead of finer cut-offs, such as $PM_{2.5}$ or PM_{10}) have been previously reported in South Asia and Northeast and East Asia to assess the sources of carbonaceous particles in full size range.[11,14,20,21] To fulfill the requirement of detection limits for microscale ^{14}C measurements in different carbonaceous aerosol fractions (see section 2.3), we used a sampling collection interval of 10−14 days. After sampling, filters were put in a precombusted glass jar (150 mL) with a Teflon-lined screw cap to avoid contaminations and stored in a dark freezer room at −20 °C before analysis. Three field blank filters were collected, shipped, stored, and measured in the same way as the samples.

2.2. Carbon-Aerosol Mass Concentration. Concentrations of OC and EC were measured by a thermal-optical transmittance method with an OC/EC Carbon Aerosol Analyzer (Sunset Laboratory Inc.) following the NIOSH protocol.[22] The triplicate analysis of samples (n = 8) showed an analytical precision with relative standard deviations of 5.8%, 12.0%, and 6.0% for OC, EC, and TC, respectively. All reported OC and TC were blank-subtracted using an average filter blank (1.8 ± 1.0 $\mu g\ cm^{-2}$; n = 3). The EC blank is smaller than the limit of detection, and thus blank correction of EC is not necessary.

2.3. Radiocarbon Analysis. ^{14}C of TC was measured by online coupling of an elemental analyzer with a Mini Carbon

DOI: 10.1021/acs.est.6b00351
Environ. Sci. Technol. XXXX, XXX, XXX−XXX

Dating System (MICADAS) equipped with a gas ion source and a versatile gas interface[23] at University of Bern, Switzerland,[24] as described in detail elsewhere.[25] To remove carbonate carbon, we exposed the filters to HCl fuming in a desiccator overnight (~12 h). ^{14}C analysis of EC was carried out by online coupling the MICADAS with a Sunset Lab OC/EC analyzer, with which OC was removed from the filter sample (1.5 cm^2) by thermal−optical Swiss_4S protocol,[26] and CO_2 evolved from the EC peak is subsequently separated.[27]

^{14}C results were expressed as fractions of modern (f_M), i.e., the fraction of the $^{14}C/^{12}C$ ratio of the sample related to that of the reference year 1950.[28] f_M(EC) for each sample was further corrected by EC loss (30 ± 8% on the average) during the OC removal steps and possibly positive EC artifact from OC charring (10 ± 6% of EC on the average) as described by refs 26 and 29. For each sample, the EC yield is quantified as ratio of the initial attenuation (ATN), as monitored by the laser signal of the OC/EC analyzer and the ATN before isolating EC for ^{14}C measurement (i.e., the EC step). Charring of OC relative to EC is estimated for each thermal step as the difference of the max. ATN and the initial ATN were normalized to the initial ATN, assuming that 50% ± 15% of the charred OC is co-evolved in the EC step. The determination of EC yield and charred OC from the laser signal was conservatively assigned with a relative uncertainty of 33%, which resulted in an overall uncertainty of f_M(EC) of 4% on the average from correction for these parameters based on error propagation. f_M(TC) was corrected for field blanks. ^{14}C results in OC (f_M(OC)) were calculated indirectly according to an isotope mass balance.[13]

Nonfossil fractions of OC and EC (i.e., f_{NF}(OC) and f_{NF}(EC), respectively) were determined from their corresponding f_M values and reference values for pure nonfossil sources by $f_{NF} = f_M(\text{sample})/f_M(\text{REF})$. These reference values are estimated as 1.07 ± 0.04 and 1.10 ± 0.05 for OC and EC, respectively, by a tree-growth model with a long-term $^{14}CO_2$ measurement[30] and by assuming the biomass-burning contribution to nonfossil OC and EC is 50% and 100%, respectively. The fraction of fossil-fuel sources was calculated by $f_{FF} = 1 - f_{NF}$. Uncertainties were determined by error propagation of all individual uncertainties, including mass determination in OC and EC, ^{14}C results in OC and EC, and reference values (f_M(REF)) as well as corrections for field blanks, EC recovery, and charring. The overall uncertainties of f_{NF} were estimated to be on average 4% (i.e., ranging from 3% to 5%) for OC and 7% (i.e., ranging from 3% to 10%) for EC, and the most important contribution to their uncertainties were generally from blank corrections and EC yield corrections for OC and EC, respectively.

2.4. Back-Trajectory Analysis. The 5 day back trajectories were calculated every 6 h for the entire campaign period using the HYSPLIT (Hybrid Single-Particle Lagrangian Integrated Trajectory) model (access provided by NOAA ARL READY Web site (http://ready.arl.noaa.gov/HYSPLIT.php)). All individual trajectories were then clustered into 3 or 4 clusters for each season using HYSPLIT to provide seasonal specific information about major-air-mass origins. The seasonal variation of back trajectories was clearly characterized, with the summertime air masses mostly originating from the ocean and in other seasons from continental regions in Northeast China and Mongolia (Figure 1).

3. RESULTS AND DISCUSSION

3.1. Overview of OC and EC Concentrations. The mass concentrations of OC and EC ranged from 0.6 to 4.1 μg m^{-3} and 0.2 to 1.5 μg m^{-3}, with a mean value of 2.2 ± 1.0 and 0.7 ± 0.4 μg m^{-3}, respectively (Figure 2). OC and EC mass

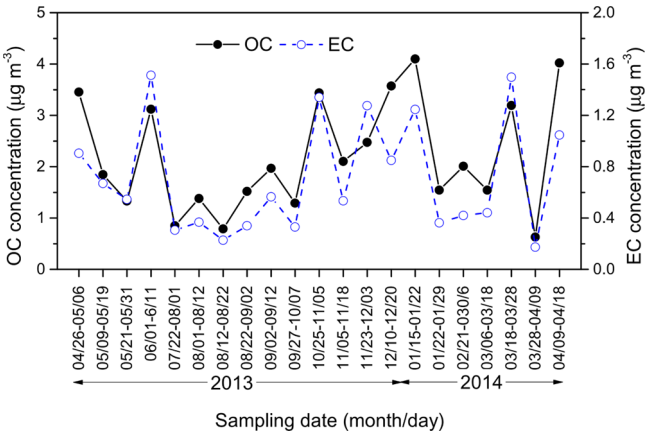

Figure 2. Temporal variations of OC and EC mass concentrations of TSP samples from Gosan.

concentrations were similar to or lower than those reported at the same site during spring and fall of 2008−2012 (excluding 2010, which had 3.3 μg m^{-3} for OC and 0.7 μg m^{-3} for EC)[31] and the ACE-Asia program during the spring of 2011 (7.00 μg m^{-3} for OC and 1.29 μg m^{-3} for EC);[32] however, our results were also much higher than those from remote sites in the North Pacific Ocean (<0.5 μg m^{-3} for OC and <0.1 μg m^{-3} for EC), with much less continental influences.[32]

The seasonal variation of carbonaceous aerosols was characterized with the lowest concentration during summer and elevated concentrations during other three seasons. The higher OC and EC loadings during these seasons were associated with significant contribution of anthropogenic air pollution outflow from Northeast China. As shown in Figure 1, air mass trajectories arriving in Gosan during spring, fall, and winter mostly passed over Mongolia and Northeast China, where high OC and EC concentrations have been often reported due to fossil-fuel combustion and biomass-burning emissions. The lower concentrations of carbonaceous aerosols during summer were attributed to "wash-out" effects with high precipitations and clean-air-mass origins from the ocean. Despite the overall low concentrations during summer, relatively high concentrations of OC and EC were observed from June 1−11, 2013. In fact, the 5 day back-trajectory analyses suggest that the air mass during this period encountered the continental regions of Japan and Korea (Figure S1), which may have increased carbonaceous aerosol concentrations by carrying the anthropogenic and biogenic emissions.

OC and EC mass concentrations reached a maximum (4.1 μg m^{-3} for OC and 1.2 μg m^{-3} for EC) during January 15−22, 2014, when the air mass passed over continental regions with a high aerosol optical depth obtained from the satellite Terra-Modis (Figure S2).[33] Furthermore, carbonaceous aerosols may have been mixed and transported with dust particles. Indeed, both OC and EC concentrations were significantly correlated ($p < 0.05$) with Ca^{2+} concentrations (Figure S3), although their regression coefficient with Ca^{2+} was much better for EC (i.e., r

DOI: 10.1021/acs.est.6b00351
Environ. Sci. Technol. XXXX, XXX, XXX−XXX

= 0.82) than for OC (i.e., r = 0.56) due to the complex sources and formation processes of OC (see sections below). Taken together, these findings suggest that the long-range transport of air masses with marine and terrestrial emissions in summer as well as fossil-fuel and biomass and biogenic emissions in the rest of the year play an important role in the abundances of carbonaceous aerosols at Gosan site. Their relative contribution of fossil fuel and biogenic and biomass emissions will be discussed in the next sections.

3.2. Source Apportionment of EC. EC is primarily produced from combustion sources. ^{14}C results (f_{NF}; see section 2.3) can be used to quantitatively determine EC mass concentrations from nonfossil biomass (EC_{NF}) and fossil fuel (EC_{FF}), and EC_{NF} is exclusively from biomass burning:

$$EC_{NF} = f_{NF}(EC) \times EC \quad (1)$$

$$EC_{FF} = EC - EC_{NF} \quad (2)$$

Source apportionment results of EC are illustrated in Figure 3. The EC_{FF} concentrations varied from 0.1 to 1.3 $\mu g\ m^{-3}$ with

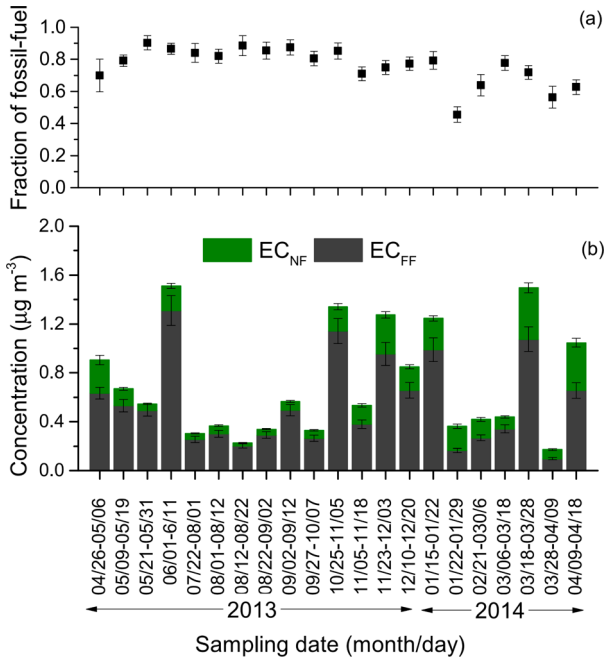

Figure 3. Temporal variations of fraction of fossil-fuel carbon in EC (a) and EC mass concentrations from nonfossil (NF) and fossil-fuel (FF) sources (b) of TSP samples from the Gosan site.

a mean of 0.55 ± 0.35 $\mu g\ m^{-3}$, which were on average 3.3 times higher than the corresponding EC_{NF} concentrations (i.e., ranging from 0.03 to 0.42 $\mu g\ m^{-3}$ with a mean of 0.16 ± 0.12 $\mu g\ m^{-3}$). The fraction of fossil to EC ranged from 40 to 83%, with an average of 76 ± 11%. This fossil contribution is comparable to those previously reported with a similar ^{14}C-based approach conduced in source regions in East China, such as a urban site of Beijing (i.e., annual average of 79 ± 6% for 2010 and 2011)[8] and a background receptor site of Ningbo (i.e., annual average of 77 ± 15% for 2009 and 2010)[34] but was much higher than that at a regional background site in South China (annual average of 25−56% for 2005 and 2006)[12] and two receptor sites in South Asia (i.e., the annual average for 2008 and 2009 was 27 ± 6% for Hanimaadhoo, Maldives and 41 ± 5% for Sinhagad, India).[20] This indicates that fossil-fuel combustion (e.g., coal combustion and vehicle emissions from East Asian continental outflow) is a dominant contributor of EC, although transported regional biomass-burning emissions (e.g., biofuel combustion and open biomass burning) could also increase the EC burden substantially.

EC_{FF} showed a positive correlation with two typical inorganic markers for fossil-fuel emissions, namely SO_4^{2-} and NO_3^- (Figure S4) due to their common sources and heterogeneous formation processes of sulfate and nitrate on the fossil-fuel-derived EC particles. Note that SO_4^{2-} and NO_3^- were not significantly correlated with EC_{NF}, fossil fuel-derived OC, and nonfossil-derived OC. It is interesting to note that the nonfossil contribution to EC was generally higher during the cold season (i.e., 31 ± 12% from November to February of the next year) than during the warm season (i.e., 21 ± 10% from March to October). This is most likely due to enhanced regional biomass-burning activities in the source regions such as Northeast China and Mongolia, especially from rural regions where biofuel combustion for domestic heating in winter is a common practice. The importance of the biomass-burning contribution during the cold period has been previously identified in Northeast China[35] and the Asian continental outflow on Okinawa Island, Japan.[36] Even in a Chinese megacity such as Beijing, the biomass-burning contribution was ~32% of the excess EC during the cold season, which was significantly higher than that during the warm period (~19%).[8]

3.3. Fossil and Nonfossil Contributions to OC. OC can be apportioned into fossil and nonfossil OC (OC_{FF} and OC_{NF}) by

$$OC_{NF} = f_{NF}(OC) \times OC \quad (3)$$

$$OC_{FF} = OC - OC_{NF} \quad (4)$$

The mass concentrations of OC_{FF} ranged from 0.2 to 2.3 $\mu g\ m^{-3}$ with an average of 0.8 ± 0.5 $\mu g\ m^{-3}$, whereas the corresponding OC_{NF} varied from 0.5 to 2.8 $\mu g\ m^{-3}$ with an average of 1.4 ± 0.7 $\mu g\ m^{-3}$ (Figure 4). In contrast to EC, OC was dominated by nonfossil sources with a mean contribution of 66 ± 11% ranging from 45 to 82%. A seasonal trend was observed for OC with higher relative and absolute fossil-fuel contributions in winter compared to summer. The winter maximum for fossil emissions was likely associated with increased coal combustion from heating in the source region of Northeast China. However, such seasonality was not observed for EC, implying an important contribution from fossil-fuel-derived SOC formation, a point discussed in the following sections. The highest relative nonfossil fraction of OC was found in late summer, which was related to less impact from transported anthropogenic aerosols (Figure 1b) and increased biogenic-derived SOC formation due to high temperature and strong solar radiation. The relative contribution from primary and secondary sources will be discussed in section 3.5.

3.4. OC and EC Ratios. The OC-to-EC ratio (OC/EC) has been frequently used as an indicator of aerosol emission sources and to estimate relative contributions of primary and secondary organic carbon.[10,37] During the sampling period, OC/EC values ranged from 1.9 to 4.8, with a mean of 3.4 ± 0.8. These results were higher than those derived from emission inventories in Korea (i.e., 1.3 for the year 2000)[38] and China (i.e., 1.67 and 1.45 for southern and northern China from 2000 to 2012),[39] implying a substantial contribution from SOC. From the ^{14}C results of OC and EC, OC and EC ratios from fossil and

DOI: 10.1021/acs.est.6b00351
Environ. Sci. Technol. XXXX, XXX, XXX−XXX

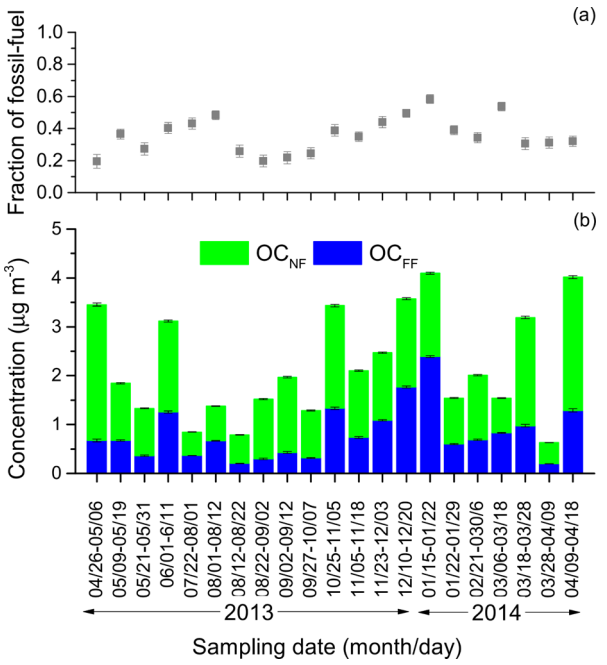

Figure 4. Temporal variations of the fraction of fossil-fuel OC in total OC (a) and OC mass concentrations from nonfossil and fossil-fuel sources (b) of TSP samples from the Gosan site.

nonfossil sources (OC_{FF}/EC_{FF} and OC_{NF}/EC_{NF}) were derived separately (Figure 5). For all of the samples, OC_{NF}/EC_{NF} was higher than OC_{FF}/EC_{FF}, which is consistent with the fact that OC/EC emission ratio values from biomass burning (i.e., 4−13 in regions dominated by biomass burning) are generally higher than those from fossil-fuel emissions (i.e., 2.6−3.6 for fossil-fuel-dominated aerosols in Chinese urban cities).[40,41]

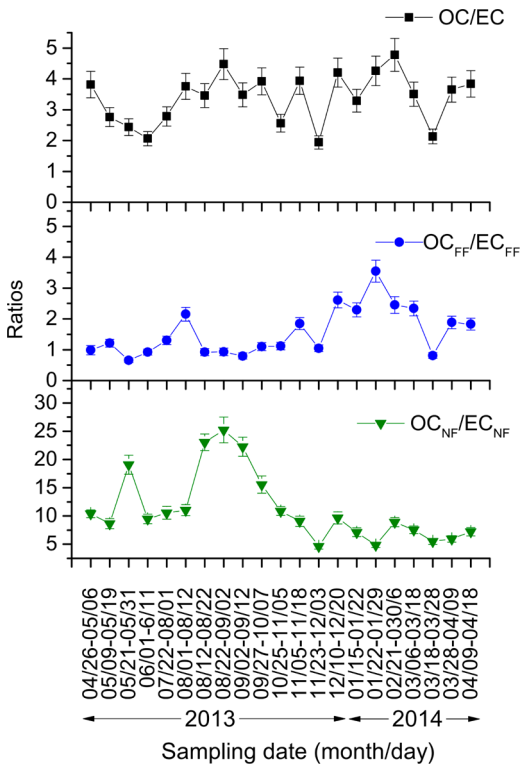

Figure 5. Temporal variations of OC-to-EC ratios (OC/EC) and mass concentration ratios of fossil-fuel (FF) carbon to nonfossil (NF) carbon (OC_{FF}/EC_{FF} and OC_{NF}/EC_{NF}) of TSP samples from the Gosan site.

Interestingly, a pronounced but different seasonal trend was found for OC_{FF}/EC_{FF} and OC_{NF}/EC_{NF}. OC_{FF}/EC_{FF} during winter (i.e., 2.7 ± 0.5) was significantly ($p < 0.01$) higher than that in the rest of the year (i.e., 1.4 ± 0.5), which may have been associated with enhanced SOC formed from fossil fuel-derived volatile organic compounds (VOCs) and increased coal combustion with higher OC/EC ratios (i.e., 1.5−15) compared to those from traffic-related emissions (i.e., 0.5−1.3).[1,42] In contrast, OC_{NF}/EC_{NF} started to increase from spring and reached the maximum during the summer, which is likely caused by enhanced biogenic-derived SOC formation and primary biogenic emissions with enriched OC particles.

3.5. Advanced ^{14}C-Based Source Apportionment of OC. An advanced ^{14}C source apportionment model was used to estimate OC concentrations from each source, which was achieved by the LHS using the data set from mass concentrations of OC and EC, estimated primary emission ratios for fossil fuel and biomass burning as well as ^{14}C results.[8] This LHS methodology is similar to the Monte Carlo simulations as described elsewhere.[8] Briefly, central (median) values with low and high limits are associated with all uncertain input parameters. All combinations of parameters are included in frequency distributions of possible solutions except those producing negative values.

First, OC_{FF} was divided into two subfractions, primary and secondary OC from fossil fuel sources, i.e., POC_{FF} and SOC_{FF}, respectively:

$$SOC_{FF} = OC_{FF} - POC_{FF} \quad (5)$$

POC_{FF} was determined from EC_{FF} and a primary OC/EC emission ratio for fossil-fuel combustion, i.e., $(POC/EC)_{FF}$:

$$POC_{FF} = EC_{FF} \times (POC/EC)_{FF} \quad (6)$$

OC_{NF} was then divided into primary biomass burning OC (POC_{BB}) and OC from other nonfossil sources (OC_{ONF}), i.e., mainly from primary biogenic OC and secondary OC from biogenic and biomass burning sources.

POC_{BB} was determined from EC_{NF} and a primary OC/EC emission ratio for biomass combustion, i.e., $(POC/EC)_{BB}$, and OC_{ONF} was subsequently calculated:

$$POC_{BB} = EC_{NF} \times (POC/EC)_{BB} \quad (7)$$

$$OC_{ONF} = OC_{NF} - POC_{BB} \quad (8)$$

Mass concentrations of source-apportioned OC (POC_{BB}, OC_{ONF}, POC_{FF}, and SOC_{FF}) are dependent on the selection of each corresponding input, such as $(POC/EC)_{FF}$ and $(POC/EC)_{BB}$. The median values of $(POC/EC)_{FF}$ and $(POC/EC)_{BB}$ amounted to 0.9 (range: 0.5−1.7) and 4.5 (3−10), respectively, according to Zhang et al.[13] and references therein. It should be noted that OC/EC values may be slightly different between coarse and fine particles. For example, Zhang et al. (2013) found that traffic-induced nonexhaust emissions and coating of EC in biomass-burning aerosols may substantially contribute to EC in coarse particles.[43] However, OC and EC emitted from traffic, coal, and biomass burning are mostly in fine fractions.[44,45] Thus, in our study we use a larger range of OC/EC values instead of a single value and discussed probabilities as shown below. Moreover, a selection of the primary OC/EC values was also comparable with the

DOI: 10.1021/acs.est.6b00351
Environ. Sci. Technol. XXXX, XXX, XXX−XXX

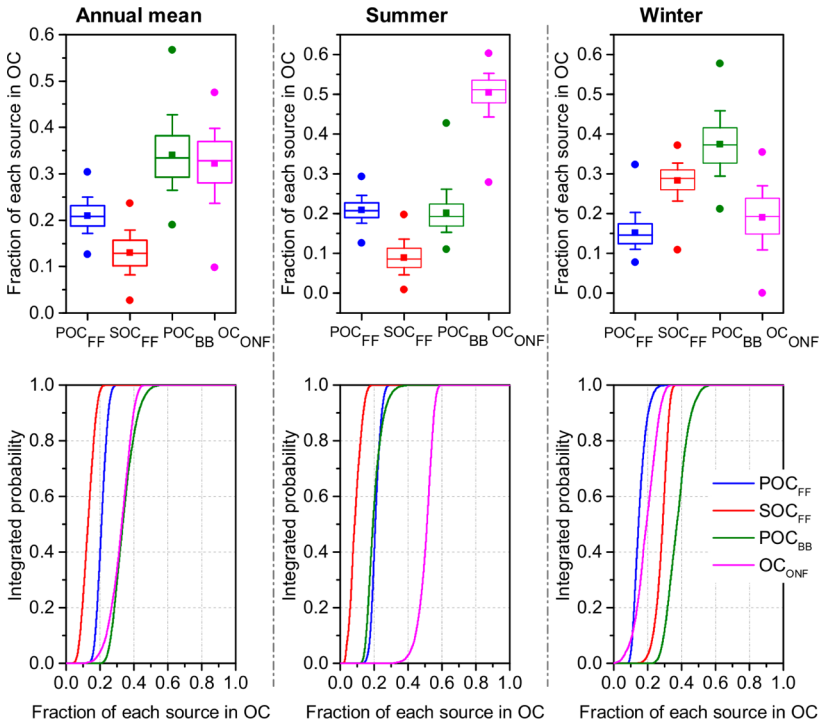

Figure 6. Fractions of each source (i.e., POC_{FF}, SOC_{FF}, POC_{BB}, and OC_{ONF}) in OC of TSP samples from Gosan and their integrated probability derived from the LHS simulations for the annual average (left column), summer (middle column), and winter (right column). The box denotes the 25th (lower line), 50th (middle line), and 75th (top line) percentiles; the solid squares within the box denote the mean values; the end of the vertical bars represents the 10th (below the box) and 90th (above the box) percentiles; and the solid dots denote maximum and minimum values. Solid curves represent the integrated probability distributions taking into account the day-to-day variability and the combined uncertainties from a full range of input parameters and measurement uncertainties. POC: primary organic carbon, SOC: secondary organic carbon, FF: fossil fuel, NF: nonfossil, ONF: other nonfossil sources.

regression slopes of OC and EC from the samples with the lowest four OC/EC values (Figure S5). Because of different $(POC/EC)_{FF}$ values for emissions from coal combustion and traffic[8,13] as mentioned above, however, the usage of a constant median value of $(POC/EC)_{FF}$ may overestimate POC_{FF} for traffic-dominated episodes based on the applied model, resulting in underestimated SOC_{FF} (and vice versa for distinct periods of coal emissions). Nevertheless, we chose a uniform $(POC/EC)_{FF}$ ratio in this work due to the lack of literature data quantifying the traffic versus coal contributions in the source regions of the air masses, which include both cities and rural areas.

To overcome the above-mentioned possible bias, we also used alternative median $(POC/EC)_{FF}$ values by decreasing and increasing the ratio by 25% assuming less and larger coal contribution in summer and winter, respectively[8] (see Figure S6 for the comparison). Furthermore, the "EC tracer method" has been often used to estimate SOC by using a minimum OC/EC value or a regression slope of OC and EC when secondary formation is not favored.[12,46,47] The "best-estimate" ratios (i.e., median) of $(POC/EC)_{FF}$ and $(POC/EC)_{BB}$ were very close to the obtained minimum OC/EC emission ratios in our experiments (i.e., 0.7 for OC_{FF}/EC_{FF} and 4.6 for OC_{NF}/EC_{NF}; see Figure 5) with negligible SOC contribution, indicating that the selections of LHS input parameters in current study is reasonable. The selectivity analysis and uncertainty estimation was conducted by varying 10 000 random combinations of input data using LHS simulations.

OC contributions from POC_{BB}, OC_{ONF}, POC_{FF}, and SOC_{FF} sources are displayed in Figure 6. On a year-round basis, the most important OC source is nonfossil OC (i.e., 66%), which is almost equally shared with primary biomass burning (i.e., 34 ± 6%) and other nonfossil sources (i.e., 32 ± 6%). The latter is mainly attributed to primary biogenic OC particles as well as SOC from atmospheric oxidation of VOCs from biogenic and biomass-burning emissions. OC_{NF} is significantly ($p < 0.05$) correlated with EC from biomass burning, implying an important contribution from primary or secondary biomass-burning sources to nonfossil fraction of OC. For fossil-fuel-derived OC, primary emissions generally predominated over secondary production with an annual averaged POC_{FF}/SOC_{FF} value of 1.6 and POC_{FF}/OC_{FF} value of 0.62.

Because contrasting seasonal trends were observed between summer and winter (see section 3.4 and Figure 5), OC source apportionment was carried out separately for these two seasons. During summer, SOC_{FF} was a minor contributor (9 ± 4%) to OC because a dramatic decrease in SOC formation from the oxidation of fossil-fuel-derived precursors occurred due to the air-mass transport from clean source regions (see Figure 1). A large fraction of summertime OC_{FF} may be from local sources without intensive aging and oxidation. Pavuluri et al. (2013) also found that a typical fossil-fuel-derived SOC tracer (i.e., 2, 3-dihydroxy-4-oxopentanoic acid) was much lower in the summer than in the winter over the outflow regions of Northeast Asia,[11] which was consistent with our findings. It should be noted that different $(POC/EC)_{FF}$ values for emissions from coal combustion and traffic discussed above may introduce a bias on seasonal SOC_{FF} changes if the coal emissions are subject to a seasonality. Nevertheless, the general observation of minor SOC_{FF} during summer and important

DOI: 10.1021/acs.est.6b00351
Environ. Sci. Technol. XXXX, XXX, XXX−XXX

SOC_{FF} during winter still remains according to Figure 6, even if the absolute values change slightly (see Figure S6). OC_{ONF} became the most important source of summertime OC, with a mean contribution of 51 ± 6%, which most likely corresponds to increased primary and secondary biogenic emissions.

During winter, OC was dominated by primary biomass burning and SOC from fossil-fuel emissions, which was associated with transported gaseous and particulate pollution from Northeast China with enhanced biomass and fossil-fuel combustions. SOC_{FF} was significantly increased during winter, which was 2 times higher than POC_{FF}. Furthermore, the occurrence of OC_{ONF} may be mainly assigned to the increase of SOC formation from nonfossil sources mainly emitted from biomass burning because biogenic-derived SOC should be small due to low ambient temperatures in winter.[48] Therefore, total SOC can be estimated as the sum of SOC_{FF} and OC_{ONF}, which accounts for 48 ± 7% of total OC, demonstrating the importance of secondary formation to the wintertime OC burden at the Gosan site. It should be noted that this can be an upper estimate of SOC because primary biogenic particles may have a minor contribution to TSP particles, even during the winter. The enhanced SOC formation in winter has been recently underlined in source regions of China.[13,49]

Given the wide range of input parameters used in the simulation, integrated probability distribution was also obtained as shown in Figure 6. Despite the fact that the large variation resulted from possibly combined solutions, the important fractions of SOC_{FF} and POC_{BB} in winter and OC_{ONF} in summer can be clearly identified and would not change almost for all possible solutions, which can therefore underscore the robustness of our results obtained in this study. The present results provide better constraints on sources and formation processes of carbonaceous aerosols in East Asia, which may be implemented into model studies to obtain a better understanding of reginal air quality and aerosol-associated climate effects. This study also demonstrates that ^{14}C measurement, along with OC and EC concentrations, emission ratios, and the LHS as well as air mass trajectory, can be used as a powerful tool to constrain the fossil versus nonfossil and primary versus secondary pollution sources of carbonaceous aerosols in the atmosphere, which can be applied in other regions in future.

■ ASSOCIATED CONTENT

Supporting Information

The Supporting Information is available free of charge on the ACS Publications website at DOI: 10.1021/acs.est.6b00351.

Figures showing air-mass backward trajectories; aerosol optical depth maps; the relationship OC and EC with Ca^{2+} concentrations; NO_3^- and SO_4^{2-} concentrations as a function of EC concentrations; scatter plots of OC and EC from fossil and nonfossil sources; and a comparison of average contributions to OC from different sources. (PDF)

■ AUTHOR INFORMATION

Corresponding Authors

*Y.-L.Z. e-mail: dryanlinzhang@gmail.com.

*K.K. phone: 81-11-706-5457; fax: 81-11-706-7142; e-mail: kawamura@lowetem.hokudai.ac.jp.

Notes

The authors declare no competing financial interest.

■ ACKNOWLEDGMENTS

We acknowledge the financial support by the Japan Society for the Promotion of Science (JSPS) (Grant-in-Aid nos. 1920405 and 24221001); the Swiss National Science Foundation; the Natural Science Foundation for Young Scientists of Jiangsu Province, China (BK20150895); and the Startup Foundation for Introducing Talent of NUIST (nos. 2015r023 and 2015r019).

■ REFERENCES

(1) Gelencsér, A.; May, B.; Simpson, D.; Sánchez-Ochoa, A.; Kasper-Giebl, A.; Puxbaum, H.; Caseiro, A.; Pio, C.; Legrand, M. Source apportionment of PM2.5 organic aerosol over Europe: Primary/secondary, natural/anthropogenic, and fossil/biogenic origin. *J. Geophys. Res.* **2007**, *112* (D23), D23S04.

(2) Jimenez, J. L.; Canagaratna, M. R.; Donahue, N. M.; Prevot, A. S. H.; Zhang, Q.; Kroll, J. H.; DeCarlo, P. F.; Allan, J. D.; Coe, H.; Ng, N. L.; Aiken, A. C.; Docherty, K. S.; Ulbrich, I. M.; Grieshop, A. P.; Robinson, A. L.; Duplissy, J.; Smith, J. D.; Wilson, K. R.; Lanz, V. A.; Hueglin, C.; Sun, Y. L.; Tian, J.; Laaksonen, A.; Raatikainen, T.; Rautiainen, J.; Vaattovaara, P.; Ehn, M.; Kulmala, M.; Tomlinson, J. M.; Collins, D. R.; Cubison, M. J.; Dunlea, E. J.; Huffman, J. A.; Onasch, T. B.; Alfarra, M. R.; Williams, P. I.; Bower, K.; Kondo, Y.; Schneider, J.; Drewnick, F.; Borrmann, S.; Weimer, S.; Demerjian, K.; Salcedo, D.; Cottrell, L.; Griffin, R.; Takami, A.; Miyoshi, T.; Hatakeyama, S.; Shimono, A.; Sun, J. Y.; Zhang, Y. M.; Dzepina, K.; Kimmel, J. R.; Sueper, D.; Jayne, J. T.; Herndon, S. C.; Trimborn, A. M.; Williams, L. R.; Wood, E. C.; Middlebrook, A. M.; Kolb, C. E.; Baltensperger, U.; Worsnop, D. R. Evolution of organic aerosols in the atmosphere. *Science* **2009**, *326* (5959), 1525−1529.

(3) Mauderly, J. L.; Chow, J. C. Health effects of organic aerosols. *Inhalation Toxicol.* **2008**, *20* (3), 257−288.

(4) Highwood, E. J.; Kinnersley, R. P. When smoke gets in our eyes: The multiple impacts of atmospheric black carbon on climate, air quality and health. *Environ. Int.* **2006**, *32* (4), 560−566.

(5) IPCC. *Climate Change 2013: The Physical Science Basis. Contribution of Working Group I to the Fifth Assessment Report of the Intergovernmental Panel on Climate Change*; Cambridge University Press: Cambridge, United Kingdom, 2013; p 1533.

(6) Pöschl, U. Atmospheric aerosols: composition, transformation, climate and health effects. *Angew. Chem., Int. Ed.* **2005**, *44* (46), 7520−40.

(7) Fuzzi, S.; Andreae, M. O.; Huebert, B. J.; Kulmala, M.; Bond, T. C.; Boy, M.; Doherty, S. J.; Guenther, A.; Kanakidou, M.; Kawamura, K.; Kerminen, V. M.; Lohmann, U.; Russell, L. M.; Poschl, U. Critical assessment of the current state of scientific knowledge, terminology, and research needs concerning the role of organic aerosols in the atmosphere, climate, and global change. *Atmos. Chem. Phys.* **2006**, *6*, 2017−2038.

(8) Zhang, Y. L.; Schnelle-Kreis, J.; Abbaszade, G.; Zimmermann, R.; Zotter, P.; Shen, R. R.; Schafer, K.; Shao, L.; Prevot, A. S.; Szidat, S. Source Apportionment of Elemental Carbon in Beijing, China: Insights from Radiocarbon and Organic Marker Measurements. *Environ. Sci. Technol.* **2015**, *49* (14), 8408−15.

(9) Jung, J. S.; Kawamura, K. Enhanced concentrations of citric acid in spring aerosols collected at the Gosan background site in East Asia. *Atmos. Environ.* **2011**, *45* (30), 5266−5272.

(10) Lee, M.; Song, M.; Moon, K. J.; Han, J. S.; Lee, G.; Kim, K. R. Origins and chemical characteristics of fine aerosols during the northeastern Asia regional experiment (atmospheric brown cloud east Asia regional experiment 2005). *J. Geophys. Res.* **2007**, *112* (D22), D22s29.

(11) Pavuluri, C. M.; Kawamura, K.; Uchida, M.; Kondo, M.; Fu, P. Q. Enhanced modern carbon and biogenic organic tracers in Northeast Asian aerosols during spring/summer. *J. Geophys. Res.* **2013**, *118* (5), 2362−2371.

(12) Zhang, Y.-L.; Li, J.; Zhang, G.; Zotter, P.; Huang, R.-J.; Tang, J.-H.; Wacker, L.; Prévôt, A. S. H.; Szidat, S. Radiocarbon-based source

DOI: 10.1021/acs.est.6b00351
Environ. Sci. Technol. XXXX, XXX, XXX−XXX

apportionment of carbonaceous aerosols at a regional background site on hainan Island, South China. *Environ. Sci. Technol.* **2014**, *48* (5), 2651−2659.
(13) Zhang, Y. L.; Huang, R. J.; El Haddad, I.; Ho, K. F.; Cao, J. J.; Han, Y.; Zotter, P.; Bozzetti, C.; Daellenbach, K. R.; Canonaco, F.; Slowik, J. G.; Salazar, G.; Schwikowski, M.; Schnelle-Kreis, J.; Abbaszade, G.; Zimmermann, R.; Baltensperger, U.; Prévôt, A. S. H.; Szidat, S. Fossil vs. non-fossil sources of fine carbonaceous aerosols in four Chinese cities during the extreme winter haze episode of 2013. *Atmos. Chem. Phys.* **2015**, *15* (3), 1299−1312.
(14) Kirillova, E. N.; Andersson, A.; Han, J.; Lee, M.; Gustafsson, O. Sources and light absorption of water-soluble organic carbon aerosols in the outflow from northern China. *Atmos. Chem. Phys.* **2014**, *14* (3), 1413−1422.
(15) Chen, B.; Andersson, A.; Lee, M.; Kirillova, E. N.; Xiao, Q.; Krusa, M.; Shi, M.; Hu, K.; Lu, Z.; Streets, D. G.; Du, K.; Gustafsson, O. Source forensics of black carbon aerosols from China. *Environ. Sci. Technol.* **2013**, *47* (16), 9102−8.
(16) Huebert, B. J.; Bates, T.; Russell, P. B.; Shi, G. Y.; Kim, Y. J.; Kawamura, K.; Carmichael, G.; Nakajima, T. An overview of ACE-Asia: Strategies for quantifying the relationships between Asian aerosols and their climatic impacts. *J. Geophys. Res.* **2003**, *108* (D23), 8633.
(17) Lim, S.; Lee, M.; Lee, G.; Kim, S.; Yoon, S.; Kang, K. Ionic and carbonaceous compositions of PM10, PM2.5 and PM1.0 at Gosan ABC Superstation and their ratios as source signature. *Atmos. Chem. Phys.* **2012**, *12* (4), 2007−2024.
(18) Jung, J.; Kawamura, K. Springtime carbon emission episodes at the Gosan background site revealed by total carbon, stable carbon isotopic composition, and thermal characteristics of carbonaceous particles. *Atmos. Chem. Phys.* **2011**, *11* (21), 10911−10928.
(19) Zhang, Y. L.; Kawamura, K.; Cao, F.; Lee, M. Stable carbon isotopic compositions of low-molecular-weight dicarboxylic acids, oxocarboxylic acids, α-dicarbonyls, and fatty acids: Implications for atmospheric processing of organic aerosols. *J. Geophys. Res.* **2016**, *121* (7), 3707−3717.
(20) Sheesley, R. J.; Kirillova, E.; Andersson, A.; Krusa, M.; Praveen, P. S.; Budhavant, K.; Safai, P. D.; Rao, P. S. P.; Gustafsson, O. Year-round radiocarbon-based source apportionment of carbonaceous aerosols at two background sites in South Asia. *J. Geophys. Res.* **2012**, *117*, No. D10202, DOI: 10.1029/2011JD017161.
(21) Gustafsson, O.; Krusa, M.; Zencak, Z.; Sheesley, R. J.; Granat, L.; Engstrom, E.; Praveen, P. S.; Rao, P. S.; Leck, C.; Rodhe, H. Brown clouds over South Asia: biomass or fossil fuel combustion? *Science* **2009**, *323* (5913), 495−8.
(22) Birch, M. E.; Cary, R. A. Elemental carbon-based method for monitoring occupational exposures to particulate diesel exhaust. *Aerosol Sci. Technol.* **1996**, *25* (3), 221−241.
(23) Wacker, L.; Fahrni, S. M.; Hajdas, I.; Molnar, M.; Synal, H. A.; Szidat, S.; Zhang, Y. L. A versatile gas interface for routine radiocarbon analysis with a gas ion source. *Nucl. Instrum. Methods Phys. Res., Sect. B* **2013**, *294*, 315−319.
(24) Szidat, S.; Salazar, G. A.; Vogel, E.; Battaglia, M.; Wacker, L.; Synal, H. A.; Turler, A. ^{14}C Analysis and Sample Preparation at the New Bern Laboratory for the Analysis of Radiocarbon with Ams (Lara). *Radiocarbon* **2014**, *56* (2), 561−566.
(25) Salazar, G.; Zhang, Y. L.; Agrios, K.; Szidat, S. Development of a method for fast and automatic radiocarbon measurement of aerosol samples by online coupling of an elemental analyzer with a MICADAS AMS. *Nucl. Instrum. Methods Phys. Res., Sect. B* **2015**, *361*, 163−167.
(26) Zhang, Y. L.; Perron, N.; Ciobanu, V. G.; Zotter, P.; Minguillón, M. C.; Wacker, L.; Prévôt, A. S. H.; Baltensperger, U.; Szidat, S. On the isolation of OC and EC and the optimal strategy of radiocarbon-based source apportionment of carbonaceous aerosols. *Atmos. Chem. Phys.* **2012**, *12*, 10841−10856.
(27) Agrios, K.; Salazar, G.; Zhang, Y.-L.; Uglietti, C.; Battaglia, M.; Luginbühl, M.; Ciobanu, V. G.; Vonwiller, M.; Szidat, S. Online coupling of pure O2 thermo-optical methods − 14C AMS for source apportionment of carbonaceous aerosols. *Nucl. Instrum. Methods Phys. Res., Sect. B* **2015**, *361*, 288−293.
(28) Stuiver, M.; Polach, H. A. Discussion: Reporting of 14C data. *Radiocarbon* **1977**, *19* (3), 355−363.
(29) Zotter, P.; Ciobanu, V. G.; Zhang, Y. L.; El-Haddad, I.; Macchia, M.; Daellenbach, K. R.; Salazar, G. A.; Huang, R. J.; Wacker, L.; Hueglin, C.; Piazzalunga, A.; Fermo, P.; Schwikowski, M.; Baltensperger, U.; Szidat, S.; Prévôt, A. S. H. Radiocarbon analysis of elemental and organic carbon in Switzerland during winter-smog episodes from 2008 to 2012 − Part 1: Source apportionment and spatial variability. *Atmos. Chem. Phys.* **2014**, *14* (24), 13551−13570.
(30) Mohn, J.; Szidat, S.; Fellner, J.; Rechberger, H.; Quartier, R.; Buchmann, B.; Emmenegger, L. Determination of biogenic and fossil CO_2 emitted by waste incineration based on $^{14}CO_2$ and mass balances. *Bioresour. Technol.* **2008**, *99* (14), 6471−6479.
(31) Lee, K.; Kim, Y. J.; Kang, C. H.; Kim, J. S.; Chang, L. S.; Park, K. Chemical characteristics of long-range-transported fine particulate matter at Gosan, Jeju Island, in the spring and fall of 2008, 2009, 2011, and 2012. *J. Air Waste Manage. Assoc.* **2015**, *65* (4), 445−454.
(32) Simoneit, B. R. T.; Kobayashi, M.; Mochida, M.; Kawamura, K.; Lee, M.; Lim, H. J.; Turpin, B. J.; Komazaki, Y. Composition and major sources of organic compounds of aerosol particulate matter sampled during the ACE-Asia campaign. *J. Geophys. Res.* **2004**, *109* (D19), D19s10.
(33) Acker, J. G.; Leptoukh, G. Online analysis enhances use of NASA Earth science data. *Eos, Transactions American Geophysical Union* **2007**, *88* (2), 14−17.
(34) Liu, D.; Li, J.; Zhang, Y.; Xu, Y.; Liu, X.; Ding, P.; Shen, C.; Chen, Y.; Tian, C.; Zhang, G. The use of levoglucosan and radiocarbon for source apportionment of $PM_{2.5}$ carbonaceous aerosols at a background site in East China. *Environ. Sci. Technol.* **2013**, *47* (18), 10454−61.
(35) Cao, F.; Zhang, S. C.; Kawamura, K.; Zhang, Y. L. Inorganic markers, carbonaceous components and stable carbon isotope from biomass burning aerosols in Northeast China. *Sci. Total Environ.*, DOI: 10.1016/j.scitotenv.2015.09.099, in press.
(36) Zhu, C.; Kawamura, K.; Kunwar, B. Effect of biomass burning over the western North Pacific Rim: wintertime maxima of anhydrosugars in ambient aerosols from Okinawa. *Atmos. Chem. Phys.* **2015**, *15* (4), 1959−1973.
(37) Lim, H. J.; Turpin, B. J. Origins of primary and secondary organic aerosol in Atlanta: Results' of time-resolved measurements during the Atlanta supersite experiment. *Environ. Sci. Technol.* **2002**, *36* (21), 4489−4496.
(38) Streets, D. G.; Bond, T. C.; Carmichael, G. R.; Fernandes, S. D.; Fu, Q.; He, D.; Klimont, Z.; Nelson, S. M.; Tsai, N. Y.; Wang, M. Q.; Woo, J. H.; Yarber, K. F. An inventory of gaseous and primary aerosol emissions in Asia in the year 2000. *J. Geophys. Res.* **2003**, *108* (D21), No. 8809, DOI: 10.1029/2002JD003093.
(39) Cui, H.; Mao, P.; Zhao, Y.; Nielsen, C. P.; Zhang, J. Patterns in atmospheric carbonaceous aerosols in China: emission estimates and observed concentrations. *Atmos. Chem. Phys.* **2015**, *15* (15), 8657−8678.
(40) Novakov, T.; Andreae, M. O.; Gabriel, R.; Kirchstetter, T. W.; Mayol-Bracero, O. L.; Ramanathan, V. Origin of carbonaceous aerosols over the tropical Indian Ocean: Biomass burning or fossil fuels? *Geophys. Res. Lett.* **2000**, *27* (24), 4061−4064.
(41) Zhang, X. Y.; Wang, Y. Q.; Zhang, X. C.; Guo, W.; Gong, S. L. Carbonaceous aerosol composition over various regions of China during 2006. *J. Geophys. Res.* **2008**, *113* (D14), D14111.
(42) Zhi, G.; Chen, Y.; Feng, Y.; Xiong, S.; Li, J.; Zhang, G.; Sheng, G.; Fu, J. Emission Characteristics of Carbonaceous Particles from Various Residential Coal-Stoves in China. *Environ. Sci. Technol.* **2008**, *42* (9), 3310−3315.
(43) Zhang, Y. L.; Zotter, P.; Perron, N.; Prévôt, A. S. H.; Wacker, L.; Szidat, S. Fossil and non-fossil sources of different carbonaceous fractions in fine and coarse particles by radiocarbon measurement. *Radiocarbon* **2013**, *55* (2−3), 1510−1520.

(44) Zhang, H.; Wang, S.; Hao, J.; Wan, L.; Jiang, J.; Zhang, M.; Mestl, H. E. S.; Alnes, L. W. H.; Aunan, K.; Mellouki, A. W. Chemical and size characterization of particles emitted from the burning of coal and wood in rural households in Guizhou, China. *Atmos. Environ.* **2012**, *51* (0), 94−99.
(45) Huang, X. F.; Yu, J. Z.; He, L. Y.; Hu, M. Size distribution characteristics of elemental carbon emitted from Chinese vehicles: results of a tunnel study and atmospheric implications. *Environ. Sci. Technol.* **2006**, *40* (17), 5355−60.
(46) Castro, L. M.; Pio, C. A.; Harrison, R. M.; Smith, D. J. T. Carbonaceous aerosol in urban and rural European atmospheres: estimation of secondary organic carbon concentrations. *Atmos. Environ.* **1999**, *33* (17), 2771−2781.
(47) Turpin, B. J.; Huntzicker, J. J. Identification of Secondary Organic Aerosol Episodes and Quantitation of Primary and Secondary Organic Aerosol Concentrations during Scaqs. *Atmos. Environ.* **1995**, *29* (23), 3527−3544.
(48) Ding, X.; He, Q. F.; Shen, R. Q.; Yu, Q. Q.; Zhang, Y. Q.; Xin, J. Y.; Wen, T. X.; Wang, X. M. Spatial and seasonal variations of isoprene secondary organic aerosol in China: Significant impact of biomass burning during winter. *Sci. Rep.* **2016**, *6*, 20411.
(49) Huang, R. J.; Zhang, Y.; Bozzetti, C.; Ho, K. F.; Cao, J. J.; Han, Y.; Daellenbach, K. R.; Slowik, J. G.; Platt, S. M.; Canonaco, F.; Zotter, P.; Wolf, R.; Pieber, S. M.; Bruns, E. A.; Crippa, M.; Ciarelli, G.; Piazzalunga, A.; Schwikowski, M.; Abbaszade, G.; Schnelle-Kreis, J.; Zimmermann, R.; An, Z.; Szidat, S.; Baltensperger, U.; El Haddad, I.; Prevot, A. S. High secondary aerosol contribution to particulate pollution during haze events in China. *Nature* **2014**, *514* (7521), 218−22.

DOI: 10.1021/acs.est.6b00351
Environ. Sci. Technol. XXXX, XXX, XXX−XXX